Design of an Exosuit for assistance based on physical human-robot interaction performance improvement

Yaodong Lu, Yannick Aoustin, Vigen Arakelian

Noname manuscript No.
(will be inserted by the editor)

Design of an Exosuit for assistance based on physical human-robot interaction performance improvement

Yaodong Lu · Yannick Aoustin · Vigen Arakelian

Received: date / Accepted: date

Abstract Exoskeleton robots have wide application in industrial field as well as for patients with locomotor disability. Among them, the exoskeleton with flexible structure, named exosuit has aroused great interest among researchers. They are usually made of soft material like cables and fabrics. Since there are no rigid frames and links in the Exosuits, they are much lighter and have less misalignment problems than the rigid exoskeletons. However, the physical human-robot interaction still remains a problem in the Exosuit design. Excessive pressure exerted by cables on soft tissues and skeleton of the human will lead to discomfort or even injuries. Besides, as assistive device, Exosuits are usually worn by users over a long period of time, which requires high energy efficiency. In this paper, based on these considerations, a multi-objective optimization approach based on swarm intelligence has been developped and applied in order to improve the physical human-robot interaction and energy efficiency performance of an upper-limb Exosuit for assistance. The optimization results have demonstrated its effectiveness in the design phase.

Keywords Exoskeleton · Cable-driving wearable robot modelling · Exosuit · Physical human-robot interaction · Multi-objective optimization · Energy efficiency

Yaodong Lu
LS2N, ECN-Nantes Université UMR 6004, 1 rue de la Noë, Nantes, BP 92101, F-44321, France
Tel.: +123-45-678910
Fax: +123-45-678910
E-mail: yaodong.lu@ls2n.fr

Yannick Aoustin
LS2N, ECN-Nantes Université UMR 6004, 1 rue de la Noë, Nantes, BP 92101, F-44321, France
E-mail: yannick.aoustin@univ-nantes.fr

1 Introduction

In the last decade, exoskeleton robots become one of the potential solutions for assisting the patients with locomotor disability or amplifying physical strength of workers in industrial field [10, 15]. Locomotor disability is the most commonly reported type of disability, which is defined as a person's inability to execute activities of daily living (ADL) associated with moving both himself and objects, from place to place and such inability resulting from musculoskeletal or nervous system disorders. According to a report published by the World Health Organization (WHO) [31], stroke is a leading cause of acquired disability in adults. In 2030, nearly 23 million people will suffer from stroke, which will lead to 8 million stroke deaths if secular trends continue. One-third of surviving patients from stroke do not regain their limb motor function completely. Aging of population will also aggravate the situation and increase the number of people with locomotor disabilities. As reported in [42], in France, one Frenchman by three will be aged 60 years older in 2050, who will be more likely to suffer from the locomotor disabilities. Thus, faced with these hard situations, WHO has recommended several measures enabling the people with disability more participations in the social activities and decision making. WHO has also encouraged more scientific researches on disability to improve the situation.

Assistive devices have been considered as one of the potential solutions to help the people with locomotor disabilities participate in more daily activities by amplifying their basic limb strength. To overcome the loss of lower limb extremity, the use of a wheelchair is considered as an efficient solution for the comfort and mobility of patients. According to Janssen et al. [18], upper limb assistance for every tasks is more challenging, such as bringing hands to mouth and shifting while seated. Although a robot manipulator with a robotic hand as effector could help the patients achieve their daily tasks, an upper-limb exoskeleton is more appropriate as the daily tasks could be achieved with their own dexterity. For instance, a power-assist exoskeleton robot has been developed in [23] to assist physically weak persons such as elderly, disabled, or injured person in self-rehabilitation or daily-life motions. But the kinematics of the human hand is quite complex and its behavior is quite impossible to reproduce. One important advantage of exoskeleton for upper-limb is to maintain the functionality of the human hand.

Besides, in industrial field, workers sometimes become patients suffering from work-related musculoskeletal disorders (WMSDs). Some ergonomic factors, such as physical overload, compulsive working postures and the local stiffness of definite muscle groups will lead to WMSDs. Physical overload causes the fatigue and even injury of muscles like the bicep, anterior deltoid, spinal extensor etc. To reduce the risk of WMSDs, the efficacy of exoskeleton robots has been proved in terms of physical load reduction provided [10]. For example, workers sometimes need to operate hand tools like drilling machine and welding gun for long time, which probably leads to high injury prevalence.

For static holding above the head, the exoskeleton developed in [32] brings a reduction in muscle activity for the Biceps Brachii by 30% to 70%.

This is obvious that there is a growing demand of assistive exoskeleton robots for patients with upper-limb impairment. A lot of researchers have conducted their research in the field of wearable assistive robots and several upper-limb exoskeletons have been designed for purposes ranging from physical assistance for patients [17, 23, 33, 35] to physical strength amplification of workers [1, 5, 12, 16], consisting mainly of linkages and rigid frames. It should be admitted that rigid exoskeletons show high performance for providing large forces and torques but they have several drawbacks. Large weight and inertia of rigid exoskeletons affect the mechanical transparency, which will cause fatigue and discomfort on users. Compensation technique may be one solution to this problem. For instance, the exoskeleton designed by EXAUSS company uses spring for gravity balancing. However, the additional mechanism is heavy and not easy to handle [1]. Besides, the difference in mobility between a human joint and that of a rigid exoskeleton occurs when the exoskeleton structures are oversimplified. For example, it is not sufficient to model the human shoulder joint as a 3 DOF spherical joint, which considers only the motions of glenohumeral joint. In fact, the location of glenohumeral joint is affected by the movement of shoulder girdle. Without taking this feature into account, excessive interaction force will be exerted on human due to the non-coincidence of joint axes. To solve the problem, an additional mechanism is usually designed in rigid exoskeletons to accommodate the human body movement. Schiele and Van Der Helm [39] have proposed a kinematic design, which is capable of covering the entire workspace of the human arm, including shoulder and shoulder girdle. However, the additional inertia brought by the mechanism could not be neglected and the mechanical structure becomes more complex, which is not easy to handle these problems in their design.

Avoiding the drawbacks of rigid exoskeleton, the exoskeleton with flexible structure, named exosuit has aroused great research interest. As opposed to the exoskeletons with rigid frames, they are usually fabricated with soft material like fabrics and cables and much lighter than rigid exoskeletons. Additionally, since there are no rigid joints or frames exist in exosuits, there is no problem relating to the misalignment. Mao and Agrawal [3] have proposed a design of a cable-driven arm exoskeleton for assisting and training arm movements of stroke survivors. The features like low inertia and large workspace are desirable for rehabilitation. As regards the industrial application, Zhang and Arakelian [41], Langard et al. [26] have proposed a design of upper-limb exosuit for assisting users in carrying heavy load, which possesses advantages that rigid exoskeletons do not have. In addition, to evaluate the performance of the developed exosuit in a more realistic environment and validate the simulation results, a mannequin test bench has been fabricated and tested. The test results showed that with the help of the exoskeleton, the mannequin can hold different weights of loads steadily in different postures.

In the study on the exosuit proposed in [3], the emphasis was placed on optimizing the feasible workspace of cable tension force, which is crucial for

cable actuation mechanisms. However, they did not consider the forces exerted on the user during the design phase, which could potentially result in user discomfort. The application of loads to the skeleton by upper-limb exosuit may produce excessive contact pressure, which will reduce the level of safety and comfort. Pressure magnitude and pressure distribution are related to comfort and safety. To ensure the user safety, the pressure magnitude should be lower than ischemic level (estimated at 30 mmHg), at which the capillary vessels are unable to conduct blood [25]. Another thing should be noted that not all parts of the body are suitable for transmitting loads to the skeleton. It is recommended to allow a free area around joints and to avoid areas with surface vessels or nerves, such as medical epicondyle and lateral epicondyle of upper limb [37]. Two basic strategies exist for managing an external load: concentrating the load over a small area with high pressure tolerance or distributing the load as large an area as possible. The latter could prevent the pain and injury but the comfort is not guaranteed. Goonetilleke and Eng [14] have indicated that the distribution of pressure over a large area may be less comfort for human than concentrating the pressure over a small area on the human body.

In [41] and [26], devoted to the study of upper-limb exosuit, essential attention was paid to the force exerted on the shoulder, corresponding to applying external loads over a small area with high tolerance. However, in these studies, not much attention was paid to the distribution and magnitude of the external load exerted on the soft tissues. The soft tissues transfer an important load to the skeleton and the tangential force between mechanical supports and human skin, which leads to discomfort or injury [19]. The mechanical supports must be avoided being attached to the vulnerable area or the joint movement area of upper limb. Furthermore, energy efficiency needs to be considered and improved during the design phase, as exosuits are expected to perform assistance tasks over a long period of time. Based on these considerations, it can be concluded that there is still room for further improvement in the design of upper-limb exosuit.

As discussed above, the main contribution of this paper is focused on enhancing the physical interaction and energy efficiency performance of the upper-limb exosuit. The exosuit system is modeled using static equilibrium equations. The performance in terms of physical interaction and energy efficiency is mainly influenced by design parameters such as anchor and attachment point positions. To improve the exosuit performance, an optimization problem is stated by considering as optimization variables these design parameters. A meta-heuristic algorithm is used to solve the stated optimization problem. This optimization process aims to enhance the overall performance of the exosuit system by finding the optimal values for the design parameters.

In comparison to existing studies, more exosuit performance criteria is considered in our study. Additionally, we propose an advanced optimization framework that enables efficient optimization processes by distinguishing and prioritizing different objectives in nonlinear exosuit model. Another important contribution of this work is the identification of two exosuit design parame-

ters that have the strongest positive influence on optimization criteria and constraints, which provides valuable insights in the design phase

This paper is organized as follows. Section 2, the exosuit is defined. Section 3 presents the system modeling of exosuit. Section 4, an optimization problem is stated in exosuit design. Section 5, a meta-heuristic optimization algorithm is adopted and developed. Section 6, numerical simulation and sensitivity analysis have been carried out in order to determine the most influential design parameters on the optimization criteria. Finally, section 7 offers conclusion and perspectives.

2 The Proposed exosuit

The human arm is considered as a three degrees-of-freedom (DOF) system, and the studied exosuit has four cuffs supporting the anchor points. Four cables are routed through these cuffs to actuate the exosuit, as shown in Fig. 1. They run from the anchors on upper limb and terminates at the cable winding system on the back A_i $(i = 1, 2, 3, 4)$, which are attached to the shoulder for transmitting forces. The attachment points B_i $(i = 1, 2, 3)$ on the right shoulder and B_i $(i = 4, 5, 6)$ on the left shoulder remain fixed. Their positions do not change with shoulder movement or rotation. Cable.1 runs from the anchor on point A_1 and passes through the attachment points on point B_i $(i = 1, 2, 3)$ and C_i $(i = 1, 2)$. Cable.2 runs from the anchor on point A_2 and passes through the attachment points on point B_i $(i = 1, 2, 3)$ and D_i $(i = 1, 2)$. Cable.3 runs from the anchor on point A_3 and passes through the attachment points on point B_i $(i = 1, 2, 3)$ and E_i $(i = 1, 2, 3)$. Cable.4 runs from the anchor on point A_4 and passes through the attachment points on point B_i $(i = 4, 5, 6)$ and K_i $(i = 1, 2)$.

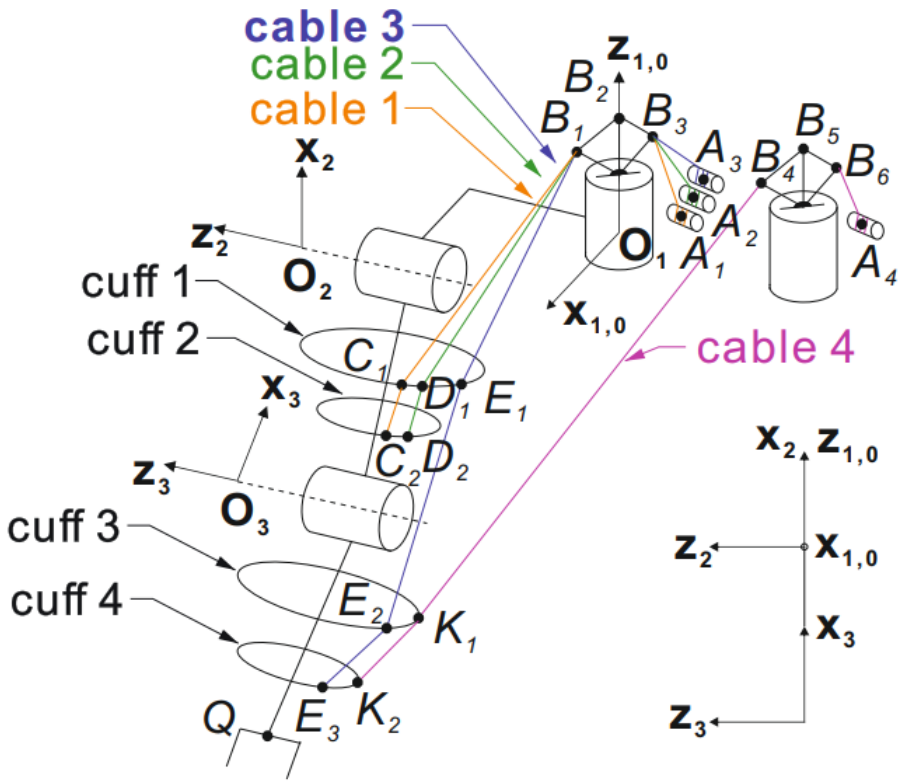

Fig. 1 Modelling of an exosuit with four cables.

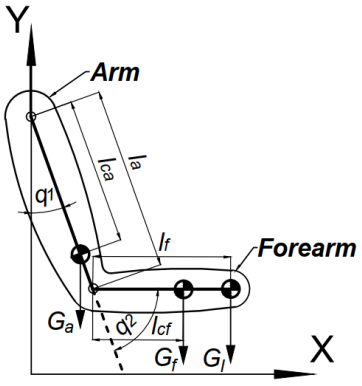

Fig. 2 Human upper-arm carrying load in the sagittal plane

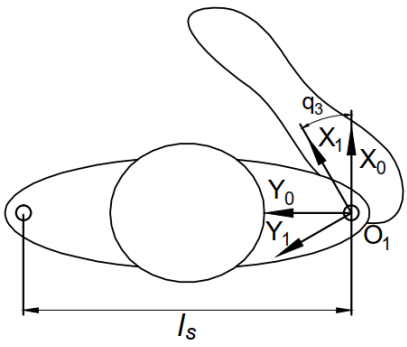

Fig. 3 Human upper-arm carrying load in the transverse plane.

The sketch of the exosuit with four cables is shown in Fig. 1. The Denavit Hartenberg modified parameters are listed in Tab. 1 [22].

Link	α_i	d_i	θ_i	r_i
1	0	0	q_1	0
2	$\pi/2$	0	$\pi/2 + q_2$	0
3	0	$-l_a$	q_3	0
4	0	$-l_f$	0	0

Table 1 Denavit Hartenberg modified parameters of human arm

3 System Modeling

When a person wants to lift and hold a certain load, one can limit oneself by studying a structure with 3 DOF (Figs. 2 and 3). To maintain certain arm configuration, the moments on the shoulder and elbow joints induced by the gravitational force can be calculated as:

$$\tau_{O_1} = \tau_{O_2} + [(m_f + m_l)gl_a + m_a g l_{ca}]\sin(q_1) \tag{1}$$

$$\tau_{O_2} = (m_f g l_{cf} + m_l g l_f)\sin(q_1 + q_2) \tag{2}$$

where m_a, m_f, and m_l are the masses of the arm, forearm, and load respectively; g is the acceleration of gravity on Earth; l_a and l_f are the lengths of arm and forearm; l_{ca} and l_{cf} denotes the locations of mass center in arm and forearm; q_1 and q_2 are the shoulder and the forearm flexion angle; q_3 is the horizontal shoulder flexion angle. In order to the user does not exert effort on the shoulder and elbow joints, a cable transmission system is introduced to compensate the gravitational forces. Let R_j $(j = 1, 2, 3)$ be the three frames attached to the two shoulder joints and to the elbow joint respectively, Fig. 1. Let us recall the (4×4) homogeneous transformation matrix ${}^i\mathbf{T}_j$ representing the transformation from frame R_i to frame R_j:

$${}^i\mathbf{T}_j = \begin{bmatrix} & {}^i\mathbf{R}_j & & {}^i\mathbf{P}_j \\ 0 & 0 & 0 & 1 \end{bmatrix} \tag{3}$$

The matrix ${}^i\mathbf{R}_j$ is (3×3) orientation matrix as follows:

$${}^i\mathbf{R}_j = \left[{}^i\mathbf{s}_j \ {}^i\mathbf{n}_j \ {}^i\mathbf{a}_j \right] \tag{4}$$

where ${}^i\mathbf{s}_j$, ${}^i\mathbf{n}_j$, and ${}^i\mathbf{a}_j$ indicate the unit vectors along the axes $\mathbf{x_j}$, $\mathbf{y_j}$, and $\mathbf{z_j}$ of the frame R_j expressed in the frame R_i. The matrix ${}^i\mathbf{T}_j$ is the matrix expressing the origin of the frame R_j in the frame R_i.

Figure 1 starting from the shoulder to the forearm, a point $\tau_{|O_2}$ defined in frame R_2 whose origin is O_2, and located on the first or the second cuff can be expressed in the reference frame R_0, whose origin O is mixed up with the origin O_1 of R_1 in the studied arm, as follows:

$$\tau = {}^0\mathbf{T}_1 {}^1\mathbf{T}_2 \tau_{|O_2} \tag{5}$$

Similarly a point $\tau_{|O_3}$ defined in frame R_3 whose origin is O_3, and located on the third or the fourth cuff can be expressed in the reference frame R_0 as follows:

$$\tau = {}^0\mathbf{T}_1\,{}^1\mathbf{T}_2\,{}^2\mathbf{T}_3\tau_{|O_3} \tag{6}$$

From (5) or (6) the virtual displacement $\delta\mathbf{O_1M}$ of the point M can be defined in frame R_0 such as:

$$\delta\mathbf{O_1M} = \mathbf{J_M}\begin{bmatrix}\delta q_1\\ \delta q_2\\ \delta q_3\end{bmatrix} \tag{7}$$

where $\mathbf{J_M}$ is the (3×3) jacobian matrix. Considering that this virtual displacement (7) is due to the application of a cable tension force F that is directed with a unit vector $\mathbf{u}^*$, the principle of virtual power can be deduced:

$$\begin{aligned}\delta\omega = &\quad (F\mathbf{u}^*)^\top\cdot\delta\mathbf{O_1M}\\ &= (F\mathbf{u}^*)^\top\cdot\mathbf{J_M}\begin{bmatrix}\delta q_1\\ \delta q_2\\ \delta q_3\end{bmatrix}\\ &= \quad(\mathbf{\Gamma}^{cable})^\top\cdot\begin{bmatrix}\delta q_1\\ \delta q_2\\ \delta q_3\end{bmatrix}\end{aligned} \tag{8}$$

where $\mathbf{\Gamma}^{cable} = \mathbf{J}_\mathbf{M}^\top F\mathbf{u}^*$ is the (3×1) vector moment applied in the shoulder or elbow joint by the cable tension force F. The joints 1 and 2 are actuated by all cables, whereas the joint 3 is only actuated by cables 3 and 4.

The power principle and the expression of the moment applied by the tension of a cable to a joint enable us to assess the joint forces provided by the four cables at shoulder and elbow level.

In each cuff, due to the motor actions each cable tension force F_i $(i = 1,2,3,4)$ exerts effort moments $\mathbf{\Gamma}^{cable.i}$ (Fig 1).

– The cable 1 trough cuffs 1 and 2 applies effort moments to the joints 1 and 2 while exerting no effort on joint 3:

$$\begin{pmatrix}\tau_{z_1}^{cable.1}\\ \tau_{z_2}^{cable.1}\\ 0\end{pmatrix} = \left[\mathbf{J}_{\mathbf{C_1}}^\top(\mathbf{u}^*_{\mathbf{C_1B_1}}+\mathbf{u}^*_{\mathbf{C_1C_2}})+\mathbf{J}^\top_{\mathbf{C_2}}\mathbf{u}^*_{\mathbf{C_2C_1}}\right]F_1 \tag{9}$$

– The cable 2 trough cuffs 1 and 2 applies effort moments to the joints 1 and 2 while exerting no effort on joint 3:

$$\begin{pmatrix}\tau_{z_1}^{cable.2}\\ \tau_{z_2}^{cable.2}\\ 0\end{pmatrix} = \left[\mathbf{J}_{\mathbf{D_1}}^\top(\mathbf{u}^*_{\mathbf{D_1B_1}}+\mathbf{u}^*_{\mathbf{D_1D_2}})+\mathbf{J}^\top_{\mathbf{D_2}}\mathbf{u}^*_{\mathbf{D_2D_1}}\right]F_2 \tag{10}$$

– The cable 3 trough cuffs 1, 3, and 4 applies effort moments to the joints 1, 2, and 3:

$$\begin{pmatrix} \tau_{z_1}^{cable.3} \\ \tau_{z_2}^{cable.3} \\ \tau_{z_3}^{cable.3} \end{pmatrix} = [\ \mathbf{J}_{\mathbf{E_1}}^{\top}(\mathbf{u}_{\mathbf{E_1B_1}}^{*} + \mathbf{u}_{\mathbf{E_1E_2}}^{*}) + \mathbf{J}_{\mathbf{E_2}}^{\top}(\mathbf{u}_{\mathbf{E_2E_1}}^{*} + \mathbf{u}_{\mathbf{E_2E_3}}^{*}) + \mathbf{J}_{\mathbf{E_3}}^{\top}\mathbf{u}_{\mathbf{E_3E_2}}^{*}\ ]\, F_3 \tag{11}$$

– The cable 4 trough cuffs 3 and 4 applies effort moments to the joints 1, 2, and 3:

$$\begin{pmatrix} \tau_{z_1}^{cable.4} \\ \tau_{z_2}^{cable.4} \\ \tau_{z_3}^{cable.4} \end{pmatrix} = [\ \mathbf{J}_{\mathbf{K_1}}^{\top}(\mathbf{u}_{\mathbf{K_1B_4}}^{*} + \mathbf{u}_{\mathbf{K_1K_2}}^{*}) + \mathbf{J}_{\mathbf{K_2}}^{\top}\mathbf{u}_{\mathbf{K_2K_1}}^{*}\ ]\, F_4 \tag{12}$$

where $\mathbf{u}$ denotes the vector between two points; $\mathbf{u}^*$ denotes the unit vector; F_i $(i = 1, 2, 3, 4)$ is the ith cable tension force. Then, the moments induced by the four cables could be expressed under a concatenate form as:

$$\mathbf{\Gamma}^{cable} = \begin{bmatrix} \tau_{z_1}^{cable.1} + \tau_{z_1}^{cable.2} + \tau_{z_1}^{cable.3} + \tau_{z_1}^{cable.4} \\ \tau_{z_2}^{cable.1} + \tau_{z_2}^{cable.2} + \tau_{z_2}^{cable.3} + \tau_{z_2}^{cable.4} \\ \tau_{z_3}^{cable.3} + \tau_{z_3}^{cable.4} \end{bmatrix} = \mathbf{J}^{\top} \begin{bmatrix} F_1 \\ F_2 \\ F_3 \\ F_4 \end{bmatrix} \tag{13}$$

Let Eq. (13) be in the under concatenate following form:

$$\mathbf{\Gamma}^{cable} = \mathbf{J}^{\top}\mathbf{T} \tag{14}$$

where $\mathbf{T} = \begin{bmatrix} F_1 & F_2 & F_3 & F_4 \end{bmatrix}^{\top}$ is the 4×1 vector of cable tension force; $\mathbf{J}$ is denoted as a 4×3 Jacobian matrix relating the anchor and attachment point positions. When wearing the exosuit, the moments induced by the gravitational force $\mathbf{G} = [0\ \tau_{O_1}\ \tau_{O_2}]^{\top}$ can be compensated by the moments generated by cables. In statics, the general form can be written as:

$$\mathbf{G} = \mathbf{J}^{\top}\mathbf{T} \tag{15}$$

It can be noted that Eq. (15) is an under-determined system. The solution of cable tension force is not unique if $\mathbf{J}^{\top}\mathbf{J}$ is invertible. The general solution can be written as

$$\mathbf{T} = \overline{\mathbf{T}} + \mathbf{N}(\mathbf{J}^{\top})\mu \tag{16}$$

where, $\overline{\mathbf{T}}$ is the minimum norm solution, which is given by:

$$\overline{\mathbf{T}} = \mathbf{J}(\mathbf{J}^{\top}\mathbf{J})^{-\mathbf{1}}\mathbf{G} \tag{17}$$

$\mathbf{N}(\mathbf{J}^\top)$ is a 4×1 null space vector and μ is an arbitrary value, assuming $\mathbf{J}^\top$ is a row full-rank matrix. Considering the cable tension vector $\mathbf{T} \in [\mathbf{T_{min}}, \mathbf{T_{max}}]$, the equivalent condition is given as:

$$\begin{bmatrix} \mathbf{N}(\mathbf{J}^\top) \\ -\mathbf{N}(\mathbf{J}^\top) \end{bmatrix} \mu \geq \begin{bmatrix} \mathbf{T_{min}} - \overline{\mathbf{T}} \\ -\mathbf{T_{max}} + \overline{\mathbf{T}} \end{bmatrix} \tag{18}$$

The feasible solution of μ is characterized by a convex region bounded by eight linear inequalities on parameter μ. If there exists no feasible numerical value of μ, the constraint on the cable tension force could not be met. According [28], linear programming has been used and the sum of cable tension forces is considered as objective function. Although it provides a high computational efficiency, the continuity of cable tension forces is very poor in the planned trajectory. To resolve the problem, quadratic programming (QP) is adopted, which allows for a step-less choice of the tension level. Step-less adjustment of cable tension forces is desirable in workspace to smoothly switch between different tension levels to reduce the energy consumption [24]. Thus, the cable-tension distribution problem can be formulated as :

$$\min \quad \mathbf{f}(\mathbf{T}) = \frac{\mathbf{1}}{\mathbf{2}}(\mathbf{T} - \mathbf{T_r})^\top(\mathbf{T} - \mathbf{T_r}) \tag{19}$$

$$\mathbf{s.t.} \quad \mathbf{T_{min}} \leq \mathbf{T} + \mathbf{N}(\mathbf{J}^\top)\mu \leq \mathbf{T_{max}} \tag{20}$$

where $\mathbf{T_r}$ is a 4×1 vector of reference cable tension forces and each component should fall in $[\mathbf{T_{min}}, \mathbf{T_{max}}]$. In comparison with linear programming, the cable tension levels are step-less and achievable in exosuit workspace.

4 An optimal design of the exosuit: Statement of the optimization problem

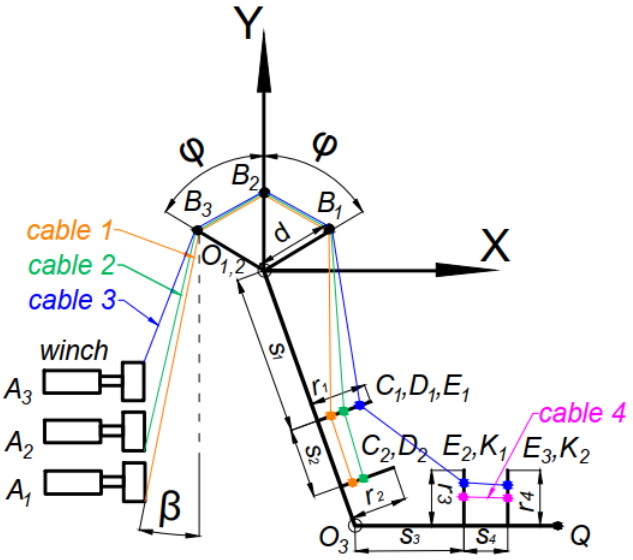

Fig. 4 Sagittal plane of exosuit

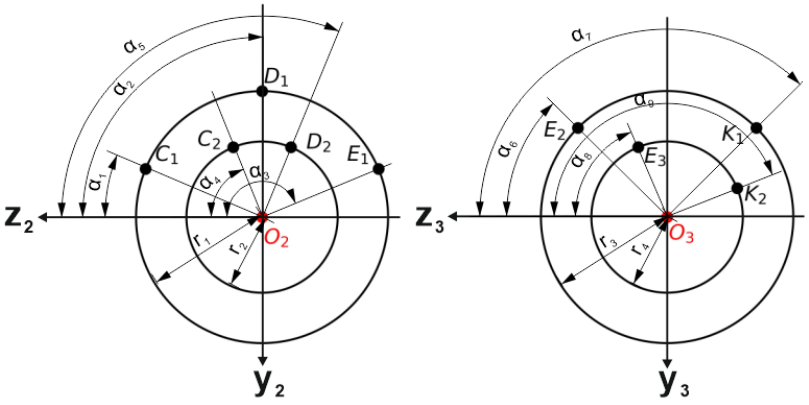

Fig. 5 Attachment points of cuffs at arm forearm

Fig. 6 Attachment points of cuffs at

The design parameters of exosuit are denoted as: s_i $(i = 1, ..., 4)$, r_i $(i = 1, ..., 4)$, α_i $(i = 1, ..., 9)$, φ, β, and d, which describe the arrangement of anchor and attachment points (see Figs. 4, 5, and 6). We assume when users carry load, their back is always upright and cable winch systems are attached to the body, ie. all the vectors to the winch $\mathbf{v_{B_3A_i}}$ $(i = 1, 2, 3)$ and $\mathbf{v_{B_6A_4}}$ are

opposed to the axis $\mathbf{z_0}$ ($\beta = 0°$). These 19 design parameters are chosen as optimization variables of the considered optimization problem.

It can be observed from Eq. (13) that the relation between cable tension forces and the moment induced by the cables on joints are determined by the optimization variables. As the same situation in cable-driven robot, the attachment points on the frame should be identified precisely for high transmission efficiency. Since exoskeleton robots are quite different from traditional robots, which have a contact area with human body, safety and comfort are considered as two critical criteria in the design process. Rocon et al. [37] have concluded that kinematic compatibility and application of loads to human are the two influencing factors for the safety and comfort. As the cables are used for transmitting loads in the exosuit system, the kinematic structure is compatible with the human body and thereby no significant misalignment exists in the joints, which contributes a lot to the safety and comfort. However, the application of loads to human raises two main concerns in the exosuit design: excessive pressure on the shoulder and incompatible force on the soft tissues of upper limb, which will probably cause injuries and discomfort and must be minimized. The force exerted on shoulder is given by:

$$\begin{aligned}\|\mathbf{F}^{\mathbf{cable}}_{\mathbf{shoulder}}\| = \|\left(\mathbf{u}^*_{\mathbf{B_1C_1}} + \mathbf{u}^*_{\mathbf{B_3A_1}}\right)F_1 + \left(\mathbf{u}^*_{\mathbf{B_1D_1}} + \mathbf{u}^*_{\mathbf{B_3A_2}}\right)F_2 + \\ \left(\mathbf{u}^*_{\mathbf{B_1E_1}} + \mathbf{u}^*_{\mathbf{B_3A_3}}\right)F_3 + \left(\mathbf{u}^*_{\mathbf{B_4K_1}} + \mathbf{u}^*_{\mathbf{B_6A_4}}\right)F_4\|\end{aligned} \tag{21}$$

Besides, it is known that the load transmission to the human skeletal system from the wearable robot is mediated by soft tissues like skin, fat, and muscle. In the exosuit design, the tangential force induced by cables will lead to friction between mechanical components and skin, which causes pain or at least discomfort [19]. In the exosuit model (see Fig. 4), the tangential forces exerted on the skin are induced from the cables, which could be expressed as the following equation:

$$\|\mathbf{F}^{\mathbf{cable}}_{\mathbf{upper\ limb}}\| = \|\mathbf{F}^{\mathbf{cable}}_{\mathbf{arm}} + \mathbf{F}^{\mathbf{cable}}_{\mathbf{forearm}}\| \tag{22}$$

where,

$$\mathbf{F}^{\mathbf{cable}}_{\mathbf{arm}} = \left[\mathbf{u}^*_{\mathbf{C_1B_1}}F_1 + \mathbf{u}^*_{\mathbf{D_1B_1}}F_2 + \left(\mathbf{u}^*_{\mathbf{E_1B_1}} + \mathbf{u}^*_{\mathbf{E_1E_2}}\right)F_3\right] \cdot \mathbf{u}^*_{\mathbf{O_3O_2}} \tag{23}$$

$$\mathbf{F}^{\mathbf{cable}}_{\mathbf{forearm}} = \left(\mathbf{u}^*_{\mathbf{E_2E_1}}F_3 + \mathbf{u}^*_{\mathbf{K_1B_4}}F_4\right) \cdot \mathbf{u}^*_{\mathbf{QO_3}} \tag{24}$$

Another objective to be considered is the energy consumption because sometimes exosuit should be worn by user over long time for industrial needs. Particularly when upper limb remains static for holding a load, energy efficiency is mainly affected by Joule effect, which describes the process where the energy of an electric current I is converted into heat as it flows through a resistance R. In electric motors, neglecting the friction, most part of the dissipated energy is due to the loss by Joule effect. To evaluate the energy loss power P, a criterion is introduced as follows:

$$P = I^2 R \tag{25}$$

For a DC motor, considering that the torque supplied by motor is proportional to the armature current, the energy-loss criterion could be similarly evaluated as follows:

$$P' = \sum_{i=1} const_i \ \tau_i^2 \tag{26}$$

$$\tau_i^2 = (F_i r_w)^2 \tag{27}$$

where τ_i $(i = 1, 2)$ is the ith actuator torque, which could be expressed by cable tension forces F_i and r_w is the ratio of the output shaft of the DC motor; $const_i$ is the ratio between the resistance of the induct circuit R of the DC motor and the square of the torque constant. In the rest of this paper this $const_i$ will be set equal to 1. It characterizes the energy that must be produced by the battery to allow the desired motion. The heat generated by Joule effect also degrades the reliability of electrical systems components [20], which should be minimized in the design process. Although energy consumption needs to be taken into account in the design of exosuit, the first priority must be given to the safety and comfort. Besides, in the optimization process, three constraints need to be taken into account:

- Cables must be always in tension, *i.e.* cable tension forces are always positive and do not exceed the limit of cable.
- The space constraints of the positions of anchors and attachment points.
- The vulnerable parts of upper limb should be avoided in the optimization (medial, lateral epicondyle and radial, ulnar styloid process).

Based on these considerations, the multi-objective optimization problem is defined as follows:

$$\mathcal{O}_1 : \frac{1}{N} \sum_{q_1} \sum_{q_2} \sum_{q_3} \left(\|\mathbf{F}^{\mathbf{cable}}_{\mathbf{shoulder}}\| + \rho \right) \longrightarrow \min_{s_1, s_2, \ldots, d} \tag{28}$$

$$\mathcal{O}_2 : \frac{1}{N} \sum_{q_1} \sum_{q_2} \sum_{q_3} \left(\|\mathbf{F}^{\mathbf{cable}}_{\mathbf{upper\ limb}}\| + \rho \right) \longrightarrow \min_{s_1, s_2, \ldots, d} \tag{29}$$

$$\mathcal{O}_3 : P'_{max} \longrightarrow \min_{1,2,\ldots,n} \tag{30}$$

where ρ is a very large value to penalize the objective function when the cable tension force is outside the available range $[T_{min},\ T_{max}]$ at certain configuration. N is the number of points discretizing the joint space and n is the number of non-dominated solutions found by multi-objective optimization. If the cable tension forces across the entire workspace are feasible, $\mathcal{O}_1$ and $\mathcal{O}_2$ denote average forces for all postures in workspace. $\mathcal{O}_3$ denotes the maximum Joule effect power in feasible workspace.

An optimization strategy is formulated: a multi-objective optimization will be first carried out to minimize $\mathcal{O}_1$ and $\mathcal{O}_2$. Then, an optimal solution, which minimizes Joule effect power, will be selected among all the non-dominated

solutions found by multi-objective optimization. Non-dominated solutions for multi-objective optimization means that there exists no feasible solution which would decrease some criterion without causing a simultaneous increase in at least one other criterion. To obtain non-dominated solutions in a constrained domain, a multi-objective optimization algorithm is presented in the next section.

5 Optimization Algorithm and Development

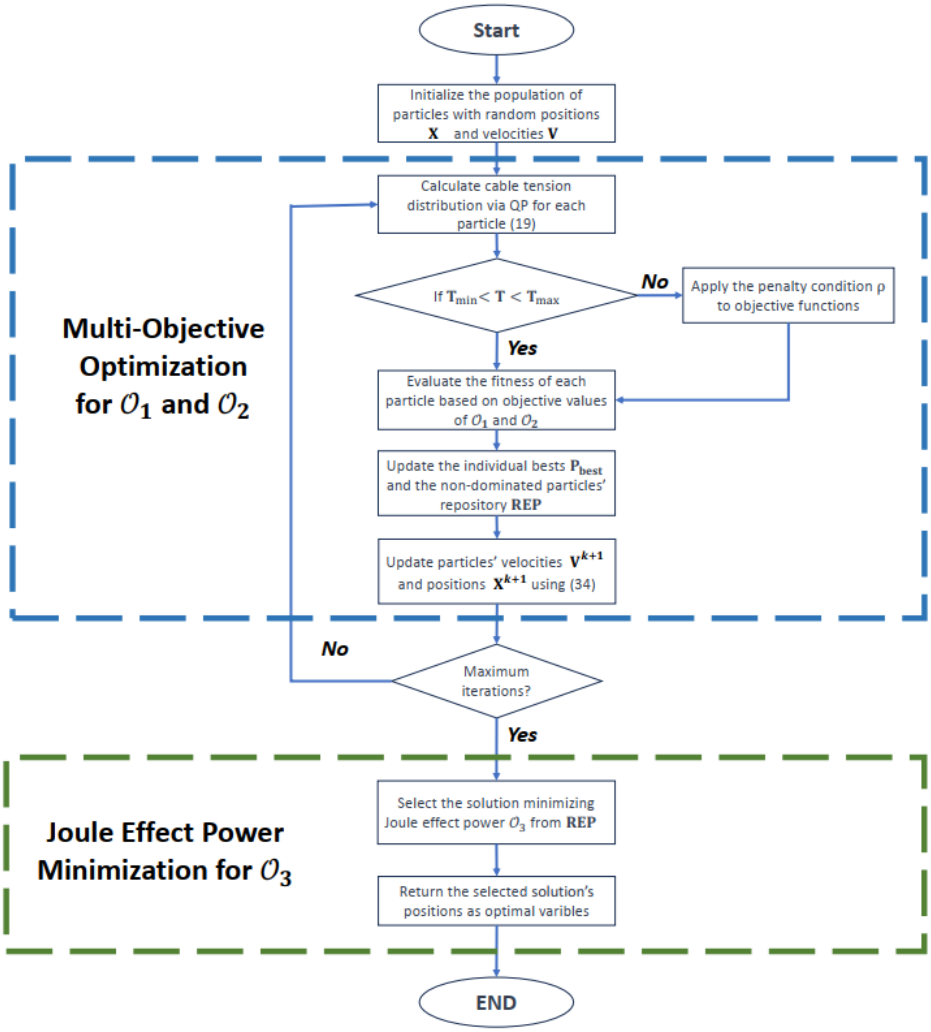

Fig. 7 Diagram of multi-objective optimization process

5.1 Inverse-PageRank-PSO

According [3,28–30], pattern search and fmincon functions via MATLAB software are adopted as optimization algorithm to improve the tension values and feasible workspace of exosuit. However, these methods may fall into the local optimum in some highly nonlinear cases. The quality of optimal solution obtained mainly depends on its initial input value. Given the highly nonlinear nature of the exosuit system described by (15), a meta-heuristic algorithm is considered as a more suitable approach. In particular, particle swarm optimization (PSO) is well-suited for multi-objective optimization mainly because of the high speed of global convergence that the algorithm presents for single-objective optimization [2,9].

PSO is a population-based metaheuristic optimization inspired by the choreography of a bird flock, which has been found to be successful in a wide variety of optimization task. To identify the design parameters of exosuit, a more efficient PSO variant, named Inverse-PageRank-PSO (I-PR-PSO), has been used [11]. I-PR-PSO is based both on the standard PSO [8,21,36] and PageRank algorithm [7,27]. By ranking the particles in a smart way, defined by an inverse PageRank strategy [11,34], this algorithm is strongly decreasing the number of iterations, and so the number of fitness calculation calls needed to obtain an optimized solution. In I-PR-PSO, as well as in the classical version of PSO, particles are defined, that are each representing a potential solution to the considered objective function. Then, these particles are flying through the research domain, by following each other in a smart way, to converge together to the global optimum of the considered objective function. To do so, the way the particles are influencing each other is considered as a Markov chain. In this way, the probability matrix can be deduced from the relative success of each particle (for more details, see [11]). Then, the links between particles, that is the way they are influencing each other, is smartly evolving as the calculation is going on, for the best particles to be the most influential upon the swarm. So, at each iteration $k+1$ of the optimization process, the speed $\mathbf{V_i^{k+1}}$ and position $\mathbf{X_i^{k+1}}$ of every particle i has to be recalculated, by using the following equations:

$$\begin{cases} \mathbf{V_i^{k+1}} = w\mathbf{V_i^k} + c_1\mathcal{R}_1(\mathbf{P_{i,best}^{k+1}} - \mathbf{X_i^k}) + c_2\mathcal{R}_2\sum_{j=1}^{n}\mathcal{C}_{ij}[\mathbf{P_{j,best}^{k+1}} - \mathbf{X_i^k}] \\ \mathbf{X_i^{k+1}} = \mathbf{X_i^k} + \mathbf{V_i^{k+1}} \end{cases} \tag{31}$$

where w is weighing the influence of the previous speed on the new one, *i.e.* is representing the inertia of particles during their movement in the research domain, c_1 and c_2 denote acceleration constants, $\mathcal{R}_1$ and $\mathcal{R}_2$ are random numbers in interval [0, 1] bestowing the heuristic characteristics of the algorithm, $\mathbf{P_{i,best}^{k+1}}$ represents the best personal position of particle i found so far. $\mathcal{C}$ is the probability transition matrix containing the coefficients weighing the influence of all the particles on the others, based on their relative success among the swarm (for more details, see [11]).

The advantage of this algorithm has been mentioned in [11]: I-PR-PSO achieves a better balance between the exploration and exploitation phases needed by the particles to find the global optimum in large dimensions. Compared to the classical PSO, the social behavior is enhanced and I-PR-PSO is more likely to find the global optimum of the considered objective function. Regarding the exosuit optimization, consisting of the identification of the attachment point positions, each particle's position $\mathbf{X_i}$ is a vector containing values of design parameters that are going to be tested among the fitness calculation.

However, it should be noticed that there are two optimization goals $\mathcal{O}_1$ and $\mathcal{O}_2$ first to be minimized in the optimization strategy formulated, which is a multi-objective optimization problem. Di Cesare et al. [11] does not provide a solution to this kind of problem.

5.2 Development for Multi-Objective Optimization

To resolve a multi-objective optimization problem, Pareto-based approaches have been considered as one of solutions [13]. They aims to find the non-dominated solutions, which constitutes a Pareto front. For example, multi-objective particle swarm optimization (MOPSO) has been proposed in [9]. In MOPSO, a repository is created and contains all the non-dominated solutions found, which may be updated in each turn. The speed of each particle can be computed using the following expression:

$$\mathbf{V_i^{k+1}} = w\mathbf{V_i^k} + c_1\mathcal{R}_1(\mathbf{P_{i,best}^{k+1}} - \mathbf{X_i^k}) + c_2\mathcal{R}_2[\mathbf{REP_h^{k+1}} - \mathbf{X_i^k}] \tag{32}$$

where $\mathbf{REP_h}$ is a non-dominated solution vector taken from the repository through the roulette wheel selection method. Instead of $\mathbf{G_{best}}$ in PSO, MOPSO selects a non-dominated vector $\mathbf{REP_h}$ from the repository to guide all the particles towards the Pareto front. Inspired from MOPSO, let us consider extending functionality of I-PR-PSO for resolving a multi-objective optimization problem. The vectors taken from repository are used to calculate the stochastic matrix $\mathcal{C}$. Since we have more than one optimization goals, several matrices $\mathcal{C}_\lambda$, are calculated with Markov chain technique. A new stochastic matrix $\mathcal{C}'$ taking all the objective functions into account, which is given by:

$$\begin{aligned} \mathcal{C}' &= \sum_{\lambda}^{n_\mathcal{O}} w_\lambda^* \mathcal{C}_\lambda, \ \lambda = 1, ..., n_\mathcal{O} \\ \sum_{\lambda}^{n_\mathcal{O}} w_\lambda^* &= 1, \ \lambda = 1, ..., n_\mathcal{O} \end{aligned} \tag{33}$$

where w_λ^* denotes the weight of each probability matrix $\mathcal{C}_\lambda$ and $n_\mathcal{O}$ denotes the number of objective functions. Hence, to compute the velocity and dis-

placement, a new expression is given as follows:

$$\begin{cases} \mathbf{V_i^{k+1}} = w\mathbf{V_i^k} + c_1\mathcal{R}_1\ (\mathbf{P_{i,best}^{k+1}} - \mathbf{X_i^k}) + c_2\mathcal{R}_2 \sum_{j=1}^{n} \mathcal{C}'_{ij}[\mathbf{P_{j,best}^{k+1}} - \mathbf{X_i^k}] \\ \mathbf{X_i^{k+1}} = \mathbf{X_i^k} + \mathbf{V_i^{k+1}} \end{cases} \tag{34}$$

Through the extension inspired from MOPSO, I-PR-PSO is capable of resolving multi-objective problems and will be then used for identifying optimal exosuit design parameters. Fig. 7 illustrates the entire optimization process. The initial positions of particles are randomly selected in a constrained domain $[\mathbf{X_{min}}, \mathbf{X_{max}}]$, which is designed to avoid the vulnerable parts of upper limb. For each particle, thier fitness values are calculated using (28) and (29) respectively. If the cable tension condition is satisfied (20), no penalty value will be added on objective functions. Otherwise, penalties are applied to the objective functions. In each iteration, the algorithm compares the objective values of each particle and selects the non-dominated particles to be stored in the repository **REP**. Subsequently, the positions and velocities of all particles are updated using (34). Upon reaching the maximum number of iterations, the position of one of the solutions stored in the repository is returned as the optimal variables, aiming to minimize the Joule effect power (30). In the following section, a numerical simulation was conducted to demonstrate the effectiveness of the proposed optimization algorithm in enhancing the performance of the exosuit.

6 Numerical simulation and sensitivity analysis

6.1 Multi-objective optimization simulation

Body segment parameters in Fig. 2 and Fig. 3 are defined as follows [26]: $l_a = 0.364$ m; $l_f = 0.299$ m; $l_{ca} = 0.182$ m; $l_{cf} = 0.1495$ m; $m_a = 2.07$ kG; $m_f = 1.7$ kG. The shoulder width l_s is 0.4 m. The load mass m_l is 0.5 kG; Radius of the winch of the DC motor shafts is defined as $r_w = 0.03$ m.

Since the exosuit is used for assisting users in carrying load with their upper limb, the range of arm configurations are specified as $q_1 \in [-30°, 30°]$, $q_2 \in [10, 70°]$ and $q_3 \in [10, 70°]$. The range of each joint angle is discretized into 10 configurations, representing an evenly spaced sequence. Hence, the entire exosuit workspace is discretized into $N = 1000$ points. The limit of cable tension force is set to be: $T_{min} = 1$ N and $T_{max} = 150$ N. Cable tension vector is calculated through QP (19), in which the reference tension vector is defined as $\mathbf{T_r} = [30\ 30\ 15\ 10]^\top$. With respect to the cable tension constraints (20), $\mathcal{O}_1$ and $\mathcal{O}_2$ are going to be minimized when a user carrying 0.5 kG loads. The ranges of optimization variables are defined as: 0.1 m $\leq d \leq$ 0.15 m; 0.12 m $\leq s_1 \leq$ 0.254 m; 0.04 m $\leq s_2 \leq$ 0.06 m; 0.12 m $\leq s_3 \leq$ 0.19 m; 0.04 m $\leq s_4 \leq$ 0.06 m; 0.08 m $\leq r_1 \leq$ 0.12 m; 0.04 m $\leq r_2 \leq$ 0.08 m; 0.08 m $\leq r_3 \leq$ 0.12 m; 0.04 m $\leq r_4 \leq$ 0.08 m; $0° \leq \alpha_1 \leq 90°$; $0° \leq \alpha_2 \leq 180°$;

$90° \leq \alpha_3 \leq 180°$; $0° \leq \alpha_4 \leq 90°$; $0° \leq \alpha_5 \leq 180°$; $90° \leq \alpha_6 \leq 270°$; $90° \leq \alpha_7 \leq 270°$; $90° \leq \alpha_8 \leq 270°$; $90° \leq \alpha_9 \leq 270°$; $0° \leq \varphi \leq 90°$.

Before optimization, the initial parameters with respect to the positions of anchors and attachment points are given as following: $\varphi = 60°$; $d = 0.125$ m; $s_1 = 0.2$ m; $s_2 = 0.05$ m; $s_3 = 0.15$ m; $s_4 = 0.05$ m; $r_1 = 0.1$ m; $r_2 = 0.06$ m; $r_3 = 0.1$ m; $r_4 = 0.06$ m; $\alpha_1 = 0°$; $\alpha_2 = 0°$; $\alpha_3 = 90°$; $\alpha_4 = 0°$; $\alpha_5 = 90°$; $\alpha_6 = 90°$; $\alpha_7 = 90°$; $\alpha_8 = 90°$; $\alpha_9 = 90°$;

As shown in Fig. 8, with initial parameters, the 95.3% of workspace is infeasible before optimization, in which the cable tensions are not permissible. Another thing must be concerned with is the force exerted on the shoulder and arms by cables. Among the rest feasible configurations in workspace, simulation results show that a large portion of force is redistributed on the shoulder and upper limb. Without considering the infeasible points, $\mathcal{O}_1$ and $\mathcal{O}_2$ represent the average forces exerted on the human body, which are 300.4133 N and 121.0393 N respectively. These values indicate significant stresses for users. Therefore, it is crucial to identify appropriate design parameters during the exosuit conception phase.

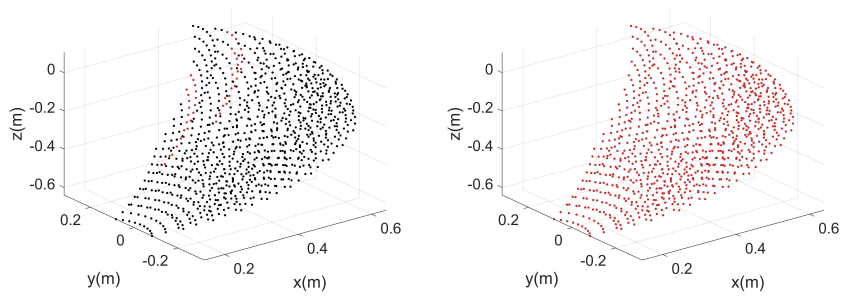

Fig. 8 Exosuit workspace before (left) and after (right) optimization. Brown dots are feasible, while black dots are infeasible.

Therefore, the multi-objective optimization process in Fig. 7 has been carried out in MATLAB software®. I-PR-PSO calculation parameters [11] were chosen as: inertial weight of particles $w = 0.8$; acceleration constants $c_1 = c_2 = 2$; number of particles $N_p = 20$; repository capacity $N_r = 20$; maximum number of I-PR-PSO iterations $r_{max} = 120$; weight of probability matrix $w_1^* = w_2^* = 0.5$. The observations showed that two fitness values of the particles, representing different design parameter combinations, converged to the Pareto front in the searching process (Fig. 11). Sixteen non-dominated solutions, minimizing $\mathcal{O}_1$ or $\mathcal{O}_2$, exist on the Pareto front (Fig. 12)).

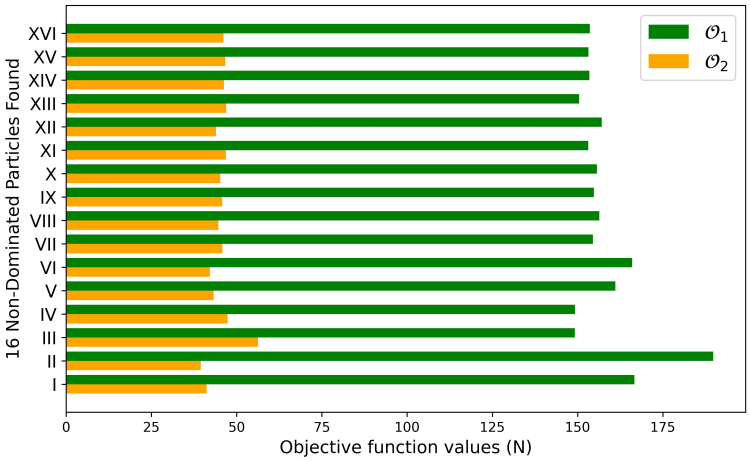

Fig. 9 $\mathcal{O}_1$ and $\mathcal{O}_2$ of 16 non-dominated solutions found by multi-objective I-PR-PSO

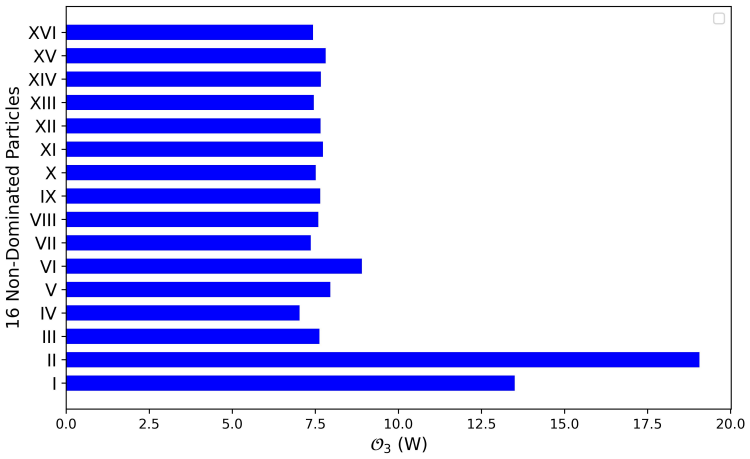

Fig. 10 $\mathcal{O}_3$ of 16 non-dominated solutions found by multi-objective I-PR-PSO

Solutions	$\mathcal{O}_1$ (N)	$\mathcal{O}_2$ (N)	$\mathcal{O}_3$ (W)
I	166.6478	41.2145	13.5021
II	189.7684	39.4642	19.0630
III	149.1851	56.2999	7.6242
IV	149.1955	47.3379	7.0246
V	161.0382	43.2853	7.9506
VI	165.9874	42.1487	8.9031
VII	154.4592	45.8034	7.3642
VIII	156.3734	44.6271	7.5888
IX	154.7761	45.7790	7.6489
X	155.6591	45.2073	7.5107
XI	153.1323	46.8366	7.7309
XII	157.0365	43.9733	7.6560
XIII	150.4569	46.9323	7.4528
XIV	153.4385	46.2937	7.6690
XV	153.1764	46.6484	7.8106
XVI	153.5888	46.1295	7.4303

Table 2 16 non-dominated solutions found by multi-objective I-PR-PSO

The objective values of the 16 non-dominated solutions are presented in Tab. 2. They are labeled with Roman numerals. As solution IV owns the minimal $\mathcal{O}_3$, it has been selected as optimal variables (see Fig. 10): $\varphi = 71.91°$; $d = 0.1500$ m; $s_1 = 0.1384$ m; $s_2 = 0.0518$ m; $s_3 = 0.1504$ m; $s_4 = 0.0489$ m; $r_1 = 0.0898$ m; $r_2 = 0.0625$ m; $r_3 = 0.1036$ m; $r_4 = 0.0582$ m; $\alpha_1 = 11.48°$; $\alpha_2 = 180°$; $\alpha_3 = 151.07°$; $\alpha_4 = 62.66°$; $\alpha_5 = 113.29°$; $\alpha_6 = 138.46°$; $\alpha_7 = 119.59°$; $\alpha_8 = 178.92°$; $\alpha_9 = 222.03°$. $\mathcal{O}_3$, the maximum Joule effect power P'_{max} for all postures is 7.0246 W. Fig. 13 and 14 illustrate the attachment point positions in exosuit with solution IV.

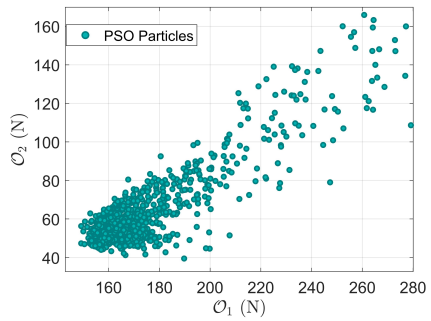

Fig. 11 Particle movement in the searching process

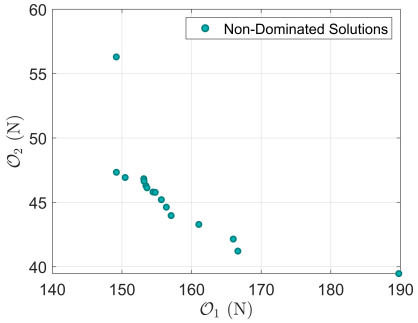

Fig. 12 Non-dominated solutions found by multi-objective I-PR-PSO

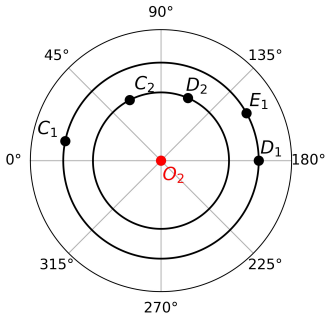

Fig. 13 Cuffs at arm with solution IV

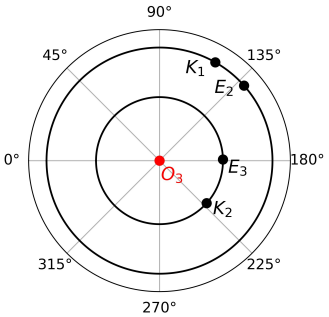

Fig. 14 Cuffs at forearm with solution IV

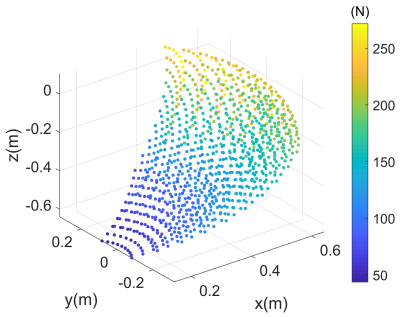

Fig. 15 Forces exerted on the shoulder by 4 cables with solution IV

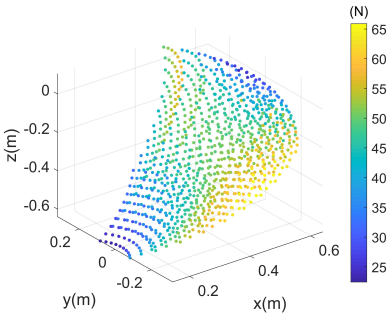

Fig. 16 Forces exerted on the upper limb by 4 cables with solution IV

Regarding the workspace, it can be observed from Fig. 8 that the feasible workspace of exosuit has been enlarged with solution IV. Due to the penalty condition set in optimization (28), the number of infeasible configurations has

been reduced to zero, which means that 4 cables are always in tension for all postures. Besides, the tension of 4 cables always fall in range $[T_{min}, T_{max}]$.

The average forces exerted on user $\mathcal{O}_1$ and $\mathcal{O}_2$ throughout the entire workspace are 149.1955 N and 47.3379 N respectively, which are more tolerable compared to the forces endured by the user before optimization. The optimized design has achieved a reduction of 50.34% and 60.89% in $\mathcal{O}_1$ and $\mathcal{O}_2$, resulting in a significant improvement in user comfort and safety.

The forces exerted on human, with respect to different postures in workspace, are presented in Figs. 15 and 16. It could be observed from the figures that the force exerted by exosuit on shoulder and upper limb also depends on user's posture. For example, the force exerted on shoulder is more than 200 N (yellow points in Fig. 15) when $z > -0.28$ m. Therefore, it is highly recommended for users to perform their tasks in postures where moderate forces are exerted on the human body, as indicated by the blue points in Figs. 15 and 16, which reduce the level of discomfort.

Regarding the tension of four cables, it is crucial to consider the continuity of forces. Poor continuity of cable tension force in the workspace can have adverse effects on the controller performance, leading to increased energy consumption and vibrations. To verify this, the exosuit workspace is discretized into 8000 points. The range of each joint angle is discretized into 20 configurations. Figs. 17-20 has shown the tension of four cables in workspace. The yellow zone in Figs. 17-20 indicates high cable tension force, while the blue zone indicates low cable tension force. Since the color variation is continuous, it can be deduced that the tension induced by four cables is step-less in the workspace. This continuity of cable tension force provides an advantage in controller design, ensuring smoother operation and improved stability.

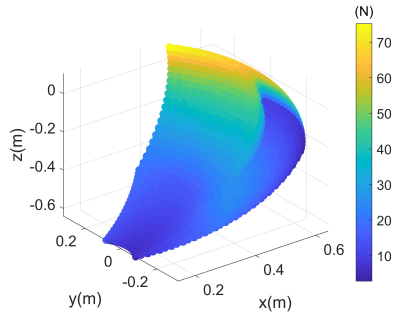

Fig. 17 Tension of cable 1 in workspace

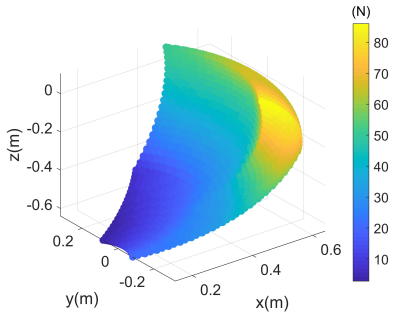

Fig. 18 Tension of cable 2 in workspace

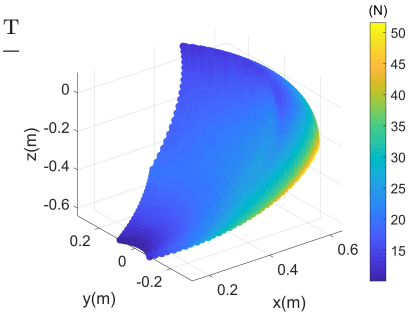

Fig. 19 Tension of cable 3 in workspace

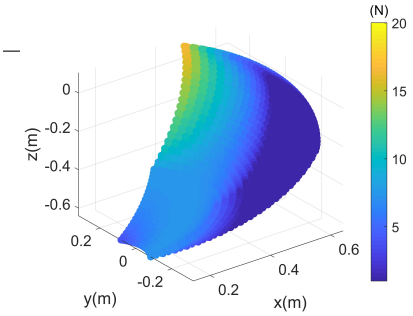

Fig. 20 Tension of cable 4 in workspace

6.2 Sensitivity analysis of design parameters

In the previous section, it has been demonstrated via numerical simulation that the proposed optimization methodology is capable of improving physical human-robot interaction and energy efficiency performance in exosuit. However, it is also necessary to identify the design parameters more affecting the physical interaction performance, which helps us enhance the understanding of exosuit model and provide valuable insights for future improvements. Taking into consideration the safety and comfort of the exosuit, obtaining information about the most influential parameter to $\mathcal{O}_1$ and $\mathcal{O}_2$ is significant during the design phase.

Global sensitivity analysis methods, like SOBOL indices [40], is attractive in dealing with non-linear systems and measuring the effect of interactions in non-additive systems. It should be admitted that these methods are capable of identifying the influential model parameters with high accuracy, but they needs a large number of sampling for each model parameter. In addition, a nonlinear model with high dimension may also lead to a high computational burden.

Given the presence of 19 design parameters in the exosuit model, a more efficient method for conducting sensitivity analysis is required. Random forest (RF), known as a stable and robust machine learning algorithm, combines the performance of numerous decision tree algorithms to classify or predict the value of a variable in a highly nonlinear model [6]. Due to the interpretability, RF is capable of providing an assessment of the relative importance of different evidential features [38], which could be applied for sensitivity analysis of design parameters. 19 design parameters in exosuit model are considered as features in RF. The sensitivity analysis stages is shown in Fig. 21:

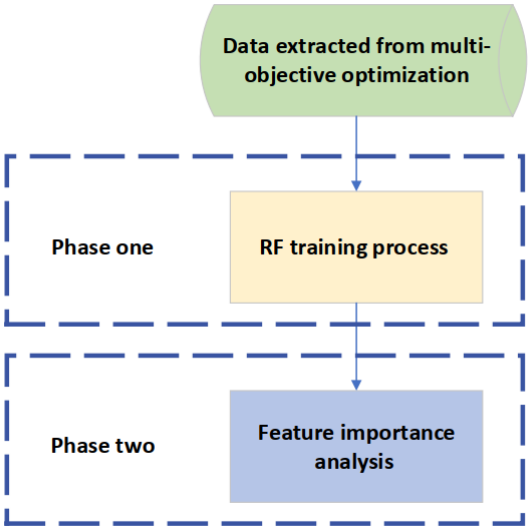

Fig. 21 Sensitivity analysis stages

A total of 985 design parameter combinations, which are available solutions throughout the entire workspace, have been extracted from the previous multi-objective optimization process. They have been split into training and testing data set (4:1). In phase one, RF is fed with training data set and a trained RF is grown. RF is made up with numerous decision trees. The principle of decision tree algorithm is to select the features which brings the maximum variance reduction. Based on these features selected in all decision trees, the trained RF could predict objective function values of testing data set. However, in our study, the trained RF is used for feature importance analysis rather than prediction of unknown data set, which is the same application described in [4].

In phase two, the importance of a feature in RF is assessed using mean decrease impurity (MDI). MDI calculates the average variance reduction $\mathcal{S}_i$ brought by that feature i in each decision tree.

$$\mathcal{S}_i = \frac{1}{N_\mathcal{D}} \sum_{j=1}^{N_\mathcal{D}} \Delta\sigma_{i,j}, \ \ j = 1, ..., N_\mathcal{D} \tag{35}$$

where $N_\mathcal{D}$ denotes the number of decision trees; $\Delta\sigma_{i,j}$ denotes the variance reduction brought by the ith feature in the jth decision tree. Training process of RF has been carried out with a Python module: scikit-learn random forest regressor. 200 decision trees are set in RF. Then, the fitting performance of trained RF is evaluated with R^2 criteria. The R^2 value are 0.7980 and 0.8053 for $\mathcal{O}_1$ and $\mathcal{O}_2$ respectively. In other words, the trained RF has explained about 80% variance of training data set. Thus, it is asserted that the trained RF is capable of expressing physical interaction model of exosuit. Feature

importance can be calculated using mean decrease impurity (MDI) to evaluate its sensitivity to interaction forces (35).

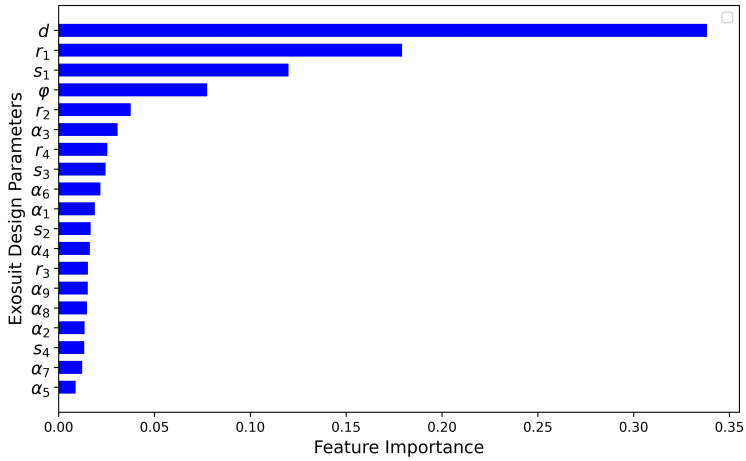

Fig. 22 Feature importance to $\mathcal{O}_1$

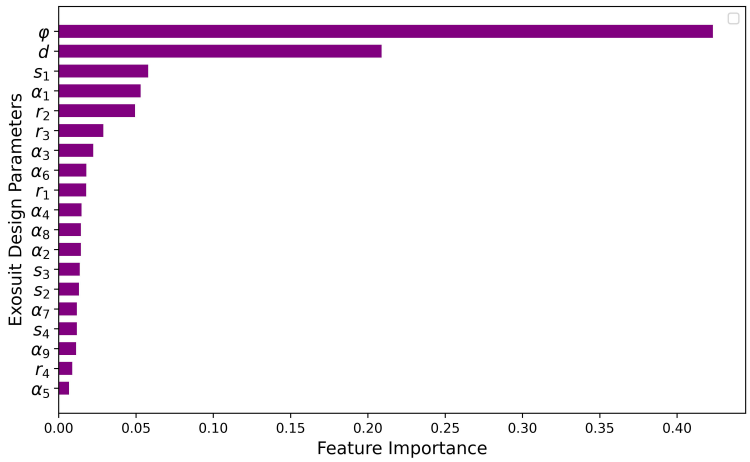

Fig. 23 Feature importance to $\mathcal{O}_2$

Observed from Figs. 22 and 23, design parameter d and φ own the most feature importance to $\mathcal{O}_1$ and $\mathcal{O}_2$ in RF respectively. In other words, the variations of d and φ contributes to most variations of objective function values respectively. They are the most sensible factors to physical human-robot interaction performance of exosuit.

During the usage of exosuit in any working condition, the anchor points should remain the position on the shoulder, with respect to d and φ, so that the forces exerted on user do not increase. It could also observed from Figs. 22

and 23 that the trained RF has also identified design parameters with less feature importance. Because they have low sensitivity to interaction forces, they can be slightly adjusted to accommodate the upper limb size of different users. In the future, it is also worth considering the possibility of reducing the dimensionality of the optimization problem by fixing parameters that have less sensitivity. By doing so, the optimization algorithm can focus on exploring the more influential parameters, increasing the possibility of discovering additional non-dominated solutions on the Pareto front within the constrained domain.

7 Conclusion and perspectives

Improvement of physical human-robot interaction performance has always been a challenge in the exosuit design. Although exosuits provide lower inertia and they have better kinematic compatibility than rigid ones, application of external loads to human body, including pressure distribution and pressure magnitude, may reduce the level of safety and comfort. Besides, as assist devices, exosuits are required to be manipulated by users for long time and thereby the energy efficiency of exosuits needs to be improved. Since there are more than one criteria to be considered in the exosuit design, a multi-objective optimization framework has been proposed to improve the performance of an upper-limb exosuit for assistance, which is based on Particle Swarm Optimization. Inverse Page-Rank Particle Swarm Optimization is a powerful PSO variant, which has been proved that it has a better global optimum searching ability than the peers. In this paper, to resolve a multi-optimization problem, the functionality of I-PR-PSO has been extended by taking the effects of all the fitness values into account. The optimization has been carried out with Matlab software and the results have demonstrated that the forces exerted on shoulder and upper limb are much less than the forces suffered by user before optimization. The feasible workspace of exosuit has been enlarged, in which the cable tension forces are continuous. Additionally, a sensitivity analysis was performed to identify the most influential parameters to physical interaction performance. This analysis contributes to a better understanding of the exosuit model and provides valuable insights for future improvements. Regarding the future work, a dimension-reduced optimization will be carried out for discovering additional non-dominated solutions on the Pareto front within the constrained domain. Considering the user safety and human-robot interaction flexibility, an appropriate controller will also be designed for actuating the exosuit system.

8 Declarations

Competing interests:

Funding: This work was supported by the China Scholarship Council [Grant Number: 202008070129].

Financial interests: The authors have no relevant financial or non-financial interests to disclose.

References

1. EXHAUSS Exosquelettes. URL https://www.exhauss.com/
2. Preface. In: J. Kennedy, R.C. Eberhart, Y. Shi (eds.) Swarm Intelligence, The Morgan Kaufmann Series in Artificial Intelligence, pp. xiii–xxvii. Morgan Kaufmann, San Francisco (2001). DOI https://doi.org/10.1016/B978-155860595-4/50000-0. URL https://www.sciencedirect.com/science/article/pii/B9781558605954500000
3. Agrawal, S.K., Dubey, V.N., Gangloff, J.J., Brackbill, E., Mao, Y., Sangwan, V.: Design and optimization of a cable driven upper arm exoskeleton. Journal of Medical Devices **3**(3) (2009)
4. Antoniadis, A., Lambert-Lacroix, S., Poggi, J.M.: Random forests for global sensitivity analysis: A selective review. Reliability Engineering & System Safety **206**, 107312 (2021)
5. Blanco, A., Catalán, J.M., Díez, J.A., García, J.V., Lobato, E., García-Aracil, N.: Electromyography assessment of the assistance provided by an upper-limb exoskeleton in maintenance tasks. Sensors **19**(15), 3391 (2019)
6. Breiman, L.: Random forests. Machine learning **45**, 5–32 (2001)
7. Brin, S., Page, L.: The anatomy of a large-scale hypertextual web search engine. Computer networks and ISDN systems **30**(1-7), 107–117 (1998)
8. Clerc, M., Kennedy, J.: The particle swarm-explosion, stability, and convergence in a multidimensional complex space. IEEE transactions on Evolutionary Computation **6**(1), 58–73 (2002)
9. Coello, C.A.C., Pulido, G.T., Lechuga, M.S.: Handling multiple objectives with particle swarm optimization. IEEE Transactions on evolutionary computation **8**(3), 256–279 (2004)
10. De Looze, M.P., Bosch, T., Krause, F., Stadler, K.S., O'sullivan, L.W.: Exoskeletons for industrial application and their potential effects on physical work load. Ergonomics **59**(5), 671–681 (2016)
11. Di Cesare, N., Chamoret, D., Domaszewski, M.: A new hybrid pso algorithm based on a stochastic markov chain model. Advances in engineering software **90**, 127–137 (2015)
12. Ebrahimi, A.: Stuttgart exo-jacket: An exoskeleton for industrial upper body applications. In: 2017 10th International Conference on Human System Interactions (HSI), pp. 258–263. IEEE (2017)
13. Fonseca, C.M., Fleming, P.J.: An overview of evolutionary algorithms in multiobjective optimization. Evolutionary computation **3**(1), 1–16 (1995)
14. Goonetilleke, R.S., Eng, T.J.: Contact area effects on discomfort. In: Proceedings of the Human Factors and Ergonomics Society Annual Meeting, vol. 38, pp. 688–690. SAGE Publications Sage CA: Los Angeles, CA (1994)
15. Gull, M.A., Bai, S., Bak, T.: A review on design of upper limb exoskeletons. Robotics **9**(1), 16 (2020). DOI 10.3390/robotics9010016. Number: 1 publisher: Multidisciplinary Digital Publishing Institute
16. Gull, M.A., Bak, T., Bai, S.: Dynamic modeling of an upper limb hybrid exoskeleton for simulations of load-lifting assistance. Proceedings of the Institution of Mechanical Engineers, Part C: Journal of Mechanical Engineering Science **236**(5), 2147–2160 (2022)
17. Gupta, A., O'Malley, M.K.: Design of a haptic arm exoskeleton for training and rehabilitation. IEEE/ASME Transactions on mechatronics **11**(3), 280–289 (2006)
18. Janssen, M.M., Bergsma, A., Geurts, A.C., De Groot, I.J.: Patterns of decline in upper limb function of boys and men with dmd: an international survey. Journal of neurology **261**(7), 1269–1288 (2014)
19. Jarrassé, N., Morel, G.: Connecting a human limb to an exoskeleton. IEEE Transactions on Robotics **28**(3), 697–709 (2011)
20. Jiao, Y., Jermsittiparsert, K., Krasnopevtsev, A.Y., Yousif, Q.A., Salmani, M.: Interaction of thermal cycling and electric current on reliability of solder joints in different solder balls. Materials Research Express **6**(10), 106302 (2019)

21. Kennedy, J., Mendes, R.: Population structure and particle swarm performance. In: Proceedings of the 2002 Congress on Evolutionary Computation. CEC'02 (Cat. No. 02TH8600), vol. 2, pp. 1671–1676. IEEE (2002)
22. Khalil, W., Dombre, E.: Modeling, identification and control of robots. Butterworth Heinemann (2002)
23. Kiguchi, K., Hayashi, Y.: An emg-based control for an upper-limb power-assist exoskeleton robot. IEEE Transactions on Systems, Man, and Cybernetics, Part B (Cybernetics) **42**(4), 1064–1071 (2012)
24. Kraus, W.: Force control of cable-driven parallel robots (2016)
25. Landis, E.M.: Micro-injection studies of capillary blood pressure in human skin. Heart **15**, 209–228 (1930)
26. Langard, M., Aoustin, Y., Arakelian, V., Chablat, D.: Investigation of the stresses exerted by an exosuit of a human arm. In: Advanced Technologies in Robotics and Intelligent Systems, pp. 425–435. Springer (2020)
27. Langville, A.N., Meyer, C.D.: Deeper inside pagerank. Internet Mathematics **1**(3), 335–380 (2004)
28. Mao, Y., Agrawal, S.K.: A cable driven upper arm exoskeleton for upper extremity rehabilitation. In: 2011 IEEE International Conference on Robotics and Automation, pp. 4163–4168. IEEE (2011)
29. Mao, Y., Agrawal, S.K.: Design of a cable-driven arm exoskeleton (carex) for neural rehabilitation. IEEE transactions on robotics **28**(4), 922–931 (2012)
30. Mao, Y., Jin, X., Dutta, G.G., Scholz, J.P., Agrawal, S.K.: Human movement training with a cable driven arm exoskeleton (carex). IEEE Transactions on Neural Systems and Rehabilitation Engineering **23**(1), 84–92 (2014)
31. Mendis, S.: Stroke disability and rehabilitation of stroke: World health organization perspective. International Journal of Stroke **8**(1), 3–4 (2013). DOI 10.1111/j.1747-4949.2012.00969.x
32. Muramatsu, Y., Kobayashi, H., Sato, Y., Jiaou, H., Hashimoto, T., Kobayashi, H.: Quantitative performance analysis of exoskeleton augmenting devices-muscle suit-for manual worker. Int. J. Autom. Technol. **5**(4), 559–567 (2011)
33. Nef, T., Riener, R.: Armin-design of a novel arm rehabilitation robot. In: 9th International Conference on Rehabilitation Robotics, 2005. ICORR 2005., pp. 57–60. IEEE (2005)
34. Newton, P.K., Mason, J., Bethel, K., Bazhenova, L.A., Nieva, J., Kuhn, P.: A stochastic markov chain model to describe lung cancer growth and metastasis. PloS one **7**(4), e34637 (2012)
35. Perry, J.C., Rosen, J., Burns, S.: Upper-limb powered exoskeleton design. IEEE/ASME transactions on mechatronics **12**(4), 408–417 (2007)
36. Reynolds, C.W.: Flocks, herds and schools: A distributed behavioral model. In: Proceedings of the 14th annual conference on Computer graphics and interactive techniques, pp. 25–34 (1987)
37. Rocon, E., Ruiz, A., Raya, R., Schiele, A., Pons, J.L., Belda-Lois, J., Poveda, R., Vivas, M., Moreno, J.: Human-robot physical interaction. Wearable robots: Biomechatronic exoskeletons pp. 127–163 (2008)
38. Rodriguez-Galiano, V., Sanchez-Castillo, M., Chica-Olmo, M., Chica-Rivas, M.: Machine learning predictive models for mineral prospectivity: An evaluation of neural networks, random forest, regression trees and support vector machines. Ore Geology Reviews **71**, 804–818 (2015)
39. Schiele, A., Van Der Helm, F.C.: Kinematic design to improve ergonomics in human machine interaction. IEEE Transactions on neural systems and rehabilitation engineering **14**(4), 456–469 (2006)
40. Sobol, I.M.: Global sensitivity indices for nonlinear mathematical models and their monte carlo estimates. Mathematics and computers in simulation **55**(1-3), 271–280 (2001)
41. Zhang, Y., Arakelian, V.: Design of a passive robotic exosuit for carrying heavy loads. in 2018 ieee-ras 18th international conference on humanoid robots (humanoids), 860–865 (2018)
42. Zhang, Y., Arakelian, V., Baron, J.: Design concepts and functional particularities of wearable walking assist devices and power-assist suits—a review. In: Proceedings of 58th international conference of machine design departments, pp. 436–41 (2017)